

Parsec - scale Herbig-Haro Outflows from Intermediate Mass Stars

F. McGroarty,¹ T.P. Ray¹ and J. Bally²

¹ Dublin Institute for Advanced Studies, 5 Merrion Square, Dublin 2, Ireland

² Department of Astrophysical and Planetary Sciences and Center for Astrophysics and Space Astronomy, University of Colorado, Campus Box 389, Boulder, CO 80309-0389, USA

Received date ;accepted date

Abstract. While there are many parsec - scale Herbig-Haro (HH) outflows known to be driven by low - mass young stars, few are associated with their intermediate mass counterparts. Here we present the discovery of five such bipolar outflows. Of these, LkH α 198, 1548C27 IRS 1, LkH α 233 and LkH α 234 were previously known to possess small-scale HH flows, while no such activity was observed before near IRAS 19395+2313. The largest of the newly discovered outflows are seen in the vicinity of LkH α 234 and 1548C27 IRS 1, and stretch (in projection) 8 pc and 7.5 pc respectively. LkH α 233 which was previously known to power a spectroscopically detected small-scale ($\leq 10''$) jet is now seen to drive a 3 pc outflow and LkH α 198 is shown here to power a 2 pc outflow. Two HH objects in the vicinity of IRAS 19395+2313 lead us to suggest that it may also be responsible for a 5 pc outflow. In total, 27 new HH objects/complexes were discovered. Examination of these parsec - scale outflows show that they have similar lengths, morphologies, and dynamical timescales as those from low - mass sources. Many appear to have blown out of the parent cloud, suggesting that their total lengths are much greater than optically observed. The degree of collimation of these outflows is similar to those from low - mass sources suggesting that the transition to more poorly - collimated outflows must occur at higher masses than the sources observed here.

Key words. ISM: Herbig-Haro objects — jets and outflows, Stars: pre-main sequence — formation, Individual — LkH α 198, 1548C27 IRS1, LkH α 233 , LkH α 234

1. Introduction

HH objects are the shock-excited nebulous tracers of outflows from pre-main sequence stars. In many cases these outflows are collimated in the form of highly supersonic jets the existence of which appear to be intrinsically linked to accretion by the underlying young stellar object (YSO) (Hartigan, Edwards, & Ghandour, 1995). Most known optical jets have low mass ($\sim 1M_{\odot}$) sources: either the embedded (IRAS Class I) counterparts of classical T Tauri stars or classical T Tauri stars themselves (Reipurth, Bally, & Devine, 1997).

Turning to higher mass YSOs ($> 10M_{\odot}$), such as those driving the Orion OMC 1 or Cepheus A outflows, one sees a very different picture (Allen & Burton, 1993; O'Dell et al., 1997; Hartigan, Morse, & Bally, 2000). Their outflows, although highly energetic, often appear poorly collimated and more chaotic (Reipurth & Bally, 2001) than their low mass counterparts. This transformation begs two obvious inter-related questions: at what point does the transition occur and is it a smooth func-

tion of mass? To answer these questions one must examine outflows from YSOs of mass greater than $\sim 2M_{\odot}$.

Optical outflows have been observed from a number of intermediate - mass ($2M_{\odot} \leq M_* \leq 10M_{\odot}$) YSOs, for example R Mon, LkH α 234, and AFGL 4029 (Ray et al., 1990 and references therein). Such stars, where optically visible, are known as Herbig Ae/Be stars (HAEBES) although their embedded counterparts have also been seen. However optical outflows from these YSOs are rare and there are a number of reasons for this. The initial mass function favours the production of low mass stars and therefore intermediate mass YSOs tend to be found at relatively large distances. More massive stars also have a faster evolutionary timescale - i.e. they evolve more quickly than low-mass YSOs and so their outflow phase is shorter. This would also make their outflows more difficult to detect. Another contributing factor could be that massive stars tend to be more obscured : intermediate and massive stars tend to be surrounded by large amounts of circumstellar gas and dust, making it harder to find an outflow at visual wavelengths. Finally there may well have been a historical bias towards studying outflows from low - mass stars. The

Send offprint requests to: F. McGroarty, fmcg@cp.dias.ie

situation however has changed in recent years as more and more studies focus on higher mass YSOs.

With these ideas in mind, we have investigated the occurrence of large-scale outflows from intermediate mass stars. By large scale we mean those stretching several parsecs e.g. the PV Cephei outflow at 2.6 pc (Gomez, Kenyon, & Whitney, 1997; Reipurth, Bally, & Devine, 1997), the HH 80/81 5.3 pc outflow (Marti, Rodriguez, & Reipurth, 1993) and the HH 354 outflow at 2.4 pc (Reipurth, Bally, & Devine, 1997). We emphasise that these outflows have vastly longer associated timescales than those of “traditionally” observed flows. A small-scale HH jet close to its source has a dynamical timescale of only a few hundred years, whereas the HH objects in these parsec-scale flows trace mass ejection over tens of thousands of years. They are, in effect, fossil records of the mass-loss histories of their parent star.

Newly detected parsec-scale outflows around five intermediate-mass young stars are discussed here (see also Table 1 and Table 2). Of these, LkH α 198, LkH α 233 and LkH α 234 are of spectral type A and 1548C27 is A7-F0. All of these stars were known to possess small-scale optical outflows. The one optically invisible YSO in our sample, IRAS 19395+2313, was not previously known to drive any outflow.

Section 2 describes how we made our observations and in Section 3 we present our newly discovered large-scale flows. The implications of our findings are discussed in Section 4 and our conclusions are drawn in Section 5.

2. Observations

To carry out our survey we used the Wide Field Camera (WFC) at the prime focus of the 2.5m Isaac Newton Telescope at El Observatorio del Roque de los Muchachos (La Palma, Canary Islands). The WFC consists of four thin-coated EEV CCDs each with 2048 x 4100 15 μ m² pixels. One pixel projects to 0".33 on the sky. Three of the CCDs are positioned from north to south with their long axes adjoining. The fourth is attached to the west to form a square mosaic (34'.2 wide) with its northwestern corner missing.

Our images were taken on nights between the 13th and the 21st of July 1998. Seeing was moderate at 1".15–1".5 as measured from the images. HH objects were identified using a number of narrowband emission line filters: H α ($\lambda_c = 6568\text{\AA}$, $\Delta\lambda(\text{FWHM}) = 95\text{\AA}$), [SII]($\lambda_c = 6725\text{\AA}$, $\Delta\lambda(\text{FWHM}) = 80\text{\AA}$) and [OIII]($\lambda_c = 5008\text{\AA}$, $\Delta\lambda(\text{FWHM}) = 100\text{\AA}$). To distinguish HH emission from reflection nebulosity, we also took broadband images in V and I. Exposure times for the narrowband and broadband images were typically 30 and 10 minutes respectively. The data was reduced using standard IRAF reduction procedures.

Object	Source	$\alpha(\text{J2000})$	$\delta(\text{J2000})$
HH 800	UNKNOWN	00 ^h 11 ^m 02.0 ^s	+58°55'04"
HH 801	LkH α 198	00 ^h 11 ^m 12.0 ^s	+58°54'01"
HH 802	LkH α 198	00 ^h 11 ^m 44.5 ^s	+58°42'39"
HH 803	1548C27 IRS 1	19 ^h 42 ^m 47.0 ^s	+23°22'19"
HH 804	IRAS 19395+2313	19 ^h 42 ^m 10.4 ^s	+23°21'49"
HH 805	IRAS 19395+2313	19 ^h 41 ^m 41.5 ^s	+23°20'34"
HH 806	UNKNOWN	19 ^h 42 ^m 03.4 ^s	+23°20'02"
HH 807	UNKNOWN	19 ^h 42 ^m 07.1 ^s	+23°19'54"
HH 808	LkH α 233	22 ^h 34 ^m 35.6 ^s	+40°39'42"
HH 809	LkH α 233	22 ^h 34 ^m 30.4 ^s	+40°39'01"
HH 810	LkH α 233	22 ^h 34 ^m 21.2 ^s	+40°37'34"
HH 811	LkH α 233	22 ^h 34 ^m 14.5 ^s	+40°36'48"
HH 812	LkH α 233	22 ^h 34 ^m 11.6 ^s	+40°36'33"
HH 813	LkH α 233	22 ^h 34 ^m 06.6 ^s	+40°36'18"
HH 814	LkH α 233	22 ^h 35 ^m 01.4 ^s	+40°43'33"
HH 815	LkH α 234	21 ^h 44 ^m 29.9 ^s	+66°13'42"
HH 816	LkH α 234	21 ^h 44 ^m 26.4 ^s	+66°10'58"
HH 817	LkH α 234	21 ^h 44 ^m 13.3 ^s	+66°10'55"
HH 818	LkH α 234	21 ^h 43 ^m 57.7 ^s	+66°10'26"
4H 819	LkH α 234	21 ^h 44 ^m 01.0 ^s	+66°09'52"
HH 820	LkH α 234	21 ^h 43 ^m 47.9 ^s	+66°09'50"
HH 821	LkH α 234	21 ^h 43 ^m 43.4 ^s	+66°08'47"
HH 103 A	LkH α 234	21 ^h 42 ^m 20.7 ^s	+66°03'31"
HH 822	LkH α 234	21 ^h 41 ^m 42.1 ^s	+66°01'45"
HH 823	UNKNOWN	21 ^h 43 ^m 27.9 ^s	+66°11'46"
HH 824	IRAS 21416+6556	21 ^h 42 ^m 56.9 ^s	+66°09'10"
HH 825	IRAS 21416+6556	21 ^h 42 ^m 39.2 ^s	+66°10'56"

Table 1. Positions of the new HH objects found in this survey and their probable sources.

3. Results for Individual Regions

3.1. LkH α 198 & V376 Cas

LkH α 198 and its nearby companion, V376 Cas, are both Herbig Ae stars (Herbig, 1960) located in the small dark cloud L1265, at a distance of 600 pc (Chavarría-K., 1985). An asymmetrical, bipolar molecular outflow in this region was noted by Canto et al. (1984). Strom et al. (1986) subsequently found the first optical outflow tracer, HH 161, a bright HH object some 12" from LkH α 198 at a position angle (P.A.) of 100°. Further observations by Goodrich (1993) yielded another HH knot 81" away at a P.A. of 153°. This object was rediscovered by Aspin & Reipurth (2000) who refer to it as HH 461.

The discovery, however, of LkH α 198 B, a deeply embedded companion to LkH α 198, by Lagage et al. (1993) raised the question of which of these two stars is the primary outflow source in this region. In their study Corcoran, Ray, & Bastien (1995) (hereafter referred to as CRB) concluded there are two separate outflows with their origin in the vicinity of LkH α 198: one driven by LkH α 198 itself and the other by LkH α 198 B. Their observations of HH 161 revealed a tail pointing back towards LkH α 198 B and they also discovered a suspected bow shock 39" south-east of this source. The bow shock (their knot B), HH 161 and its tail are all aligned and appear to constitute a one-

sided outflow from LkH α 198 B. To date no counterflow has been seen. CRB also found a number of faint HH knots (HH 164 C, D and E – see inset in Fig. 1) with the same P.A. from LkH α 198 as HH 461. Thus HH 164 C, D and E and HH 461 appears to delineate an outflow from LkH α 198. To the north they also discovered a faint knot (HH 164 F) which may be a tracer of the counterflow from LkH α 198. Finally to the east of V376 Cas a number of bright HH emission knots, HH 162, were also found by CRB. These knots were seen again in our images, although their origin remains unclear.

Two of the three HH complexes found here are extensions of the outflow from LkH α 198 discovered by CRB. HH 801 has the same P.A. of 340° with respect to LkH α 198 as HH 164 F and is therefore almost certainly part of the same flow. It appears to be an asymmetrical bow shock of which we primarily see the western wing (B in Fig. 2) some $45''$ in length. There are also a number of more easterly knots, C - F. Knot A may also be part of the western wing.

In the diametrically opposite direction from HH 801 through LkH α 198 we find HH 802. It consists of a number of features, A–I (Fig. 3) which at first sight look somewhat chaotic. Feature E, however, like its counterpart in HH 801, could be the western wing of an asymmetrical bow shock. The total length of HH 802 is some $2'$. It has a P.A. of 160° with respect to LkH α 198 and it is aligned with knots C, D and E (CRB) of HH 164 and HH 461 i.e. it is the counterflow of HH 801 and HH 164 Knot F. The furthest knot in HH 802 (Knot I) is at a distance of $8'.16$ (1.4 pc) from LkH α 198, implying the total projected extent of the flow, from HH 801 to HH 802, is some 2.3 pc.

HH 800 to the northwest of HH 801 is unlikely to be part of the HH 801 – HH 802 outflow unless the outflow direction has changed abruptly. Although changes in flow direction have been observed in other parsec-scale outflows (Reipurth & Bally, 2001), they tend to be more gradual. Moreover HH 802 is even further from LkH α 198 than HH 800 (at least in projection) and the flow associated with the former appears to have maintained a constant outflow direction. We should also add that HH 800 is probably not part of the counterflow from LkH α 198 B as its outflow is at a P.A. of 132° while HH 800 is at $\sim 330^\circ$ with respect to this source. We cannot however exclude the possibility that the outflow axis may have swung through 18° . Finally either of the two optically invisible IRAS sources in the region (Fig. 1) could be its driving source. IRAS completeness in this region is of the order of $5L_\odot$. Proper motion studies would clearly help to identify its origin.

3.2. 1548C27

The cometary-shaped reflection nebula 1548C27, and its associated H α emission line jet (HH 165) were first noted by Craine, Byard, & Boeshaar (1981). The optical jet, at a P.A. of 54° , was later confirmed by Mundt et al. (1984).

A low-mass, poorly collimated molecular outflow was also observed in the region by Dent & Aspin (1992).

Near-infrared photometry in the immediate vicinity of 1548C27 by Vilchez et al. (1989) yielded two sources. One of these appears to be a foreground star but the other, IRS 1, is located near the apex of the nebula, and they suggest this to be the driving source of HH 165 (see Fig. 4). The IRAS PSC (point source catalogue) shows IRAS 19407+2316 to be located close to, but not coincident with, IRS 1. Vilchez et al. (1989) however conclude that both near- and far-infrared sources are the same object, which, for convenience, we will refer to here as IRS 1.

The optical jet (HH 165) is very narrow, with a width of $2'' - 3''$ and its length is estimated to be $\sim 45''$. There is a gap of $\sim 13''$ between the source and the jet and two bright knots are visible at $23''$ and $29''$ from the source (Mundt et al., 1984). The kinematic distance of 1548C27 is 2.4 kpc Dent & Aspin (1992) which implies a luminosity for IRS 1 of approximately $580L_\odot$.

Another star S2, $10''$ northeast of 1548C27, was found by Scarrott, Rolph, & Tadhunter (1991). This star illuminates the nebula along with IRS 1. Scarrott, Rolph, & Tadhunter (1991) suggest HH 165 curves towards this star, implying that it is the driving source, however we find no evidence in our images to support this idea.

HH 365 to the northeast of 1548C27 was briefly referred to by Alten et al. (1997) as being bow-shaped and possibly associated with HH 165. This object was mentioned in their paper but no image of it was included. Its morphology is clearly seen here in Figs. 4 and 5. HH 365 is $8'.13$ (5.7 pc) from IRS 1 at a P.A. of 46° i.e. close to that of the HH 165 jet. From our images it appears to consist of two bright regions, Knot A and Feature B that extends to the northwest some $8''$ (Fig. 5). The overall shape of Feature B is suggestive of an asymmetrical bow, the axis of which points roughly back towards 1548C27.

Our survey also revealed a number of possible new HH objects (see Fig. 4) although several are very faint. Moreover, it is unclear whether Knots A, B and C (Fig. 6), for example, to the northwest of HH 165 are HH objects, as there is a lot of contaminating HII nebulosity in the region. However the fact that these lie on the path between HH 165 and HH 365 would suggest they might be. Further study is necessary, however, to determine their nature and for this reason we will desist from assigning them HH numbers. In any event it seems likely that HH 165 and HH 365 are part of the same outflow from IRS 1 and that Knots A, B and C may also be part of this flow.

A counterjet from IRS 1 was found recently in the near-infrared (Whelan, private communication). It lies along the same line as HH 165 at a P.A. of 234° and extends for at least $5''$. A number of faint [FeII] emitting knots were also seen beyond the counterjet. Neither the counterjet nor any of these knots are observed in our optical images, presumably because of extinction.

HH 803 (Fig. 7), 2.63 (1.85 pc) southeast of IRS 1 at a P.A. of 223° , has a very interesting morphology. It appears to be bow-shaped but convex towards IRS 1. It is $50''$ in width and contains a $13''$ “jet-like” feature bisecting the bow. The “ring” at the southern edge of the bow and the diffuse appearance of Knot A to the north add to the complexity of this object. Note that the jet-like feature does not quite point back towards IRS 1. We should also add that apart from IRS 1, no other IRAS sources were found in the region strengthening the possibility that HH 803 is driven by IRS 1.

If we include Knots A, B and C as part of the HH 165/HH 365/HH 803 outflow then its overall appearance suggests that it may be slowly precessing with shifts in the outflow direction of at least 10° . The sense of precession (i.e. point-like symmetry through IRS 1) to the northeast is also consistent with the position of HH 803 to the southwest.

3.3. The IRAS 19395+2313 Region

A number of HH objects and possible sources were found in this region (see Fig. 8), which lies approximately $18'$ west of 1548C27 and is also in the vicinity of the young open cluster NGC 6823. It is highly unlikely that any of these newly-discovered HH objects are part of the 1548C27 IRS 1 outflow although we will assume they are at the same distance, i.e. 2.4 kpc.

Two of the newly discovered HH objects are found close together - HH 806 is $30''$ west of HH 807 (Fig. 8). The region between them coincides with a gap in the CCD mosaic although a cursory inspection of the Palomar Sky Survey Red (E) plate shows there is a star in the “gap”, ALS 10422 or IRAS 19399+2312 (at $19^h42^m05.5^s +23^\circ18'59''$, J2000) which, at first sight, might be a possible HH driving source. This object is however an AGB star (Parthasarathy, Vijapurkar, & Drilling, 2000) so we can disregard it. We also see on the Palomar Sky Survey red (E) plate, a conical nebula $\sim 36''$ southeast of HH 806 (at $19^h42^m02.12^s +23^\circ19'30''$, J2000) which may be associated with the driving source of this object. In fact HH 806 lies along the major axis of this conical nebula. Although this nebula is not seen in Fig. 8, its position is marked. There is no obvious driving source for HH 807.

HH 805 has an interesting morphology (Fig. 9) and IRAS 19395+2313 seems an obvious candidate to be its driving source given its position. We have estimated the luminosity of IRAS 19395+2313 to be $\sim 320 L_\odot$. The angular extent of HH 805 is approximately $45''$ (0.5 pc) and it can be seen from Fig. 9 that this outflow is poorly collimated. Morphologically it appears to have a knotty ring-like structure and is reminiscent of the HH complex associated with V380 Ori (Corcoran & Ray, 1995). HH 804 (Fig. 8) may be part of the counterflow from IRAS 19395+2313 although we emphasise that this association is *highly* uncertain. It is at a P.A. of 80° with respect to the latter. HH 804 is at a distance of 6.3 from IRAS 19395+2313, im-

plying the total projected extent of the flow, assuming HH 804 is part of it, is ~ 5 pc.

3.4. LkH α 233

LkH α 233 is an A5e-type pre-main sequence star (Corcoran & Ray, 1997) at a distance of 880 pc and is associated with a bipolar nebula that is approximately 0.1 pc in size (Calvet & Cohen, 1978; Staude & Elsasser, 1993). The nebula has a distinct X-like morphology with bright reflection limbs at $50^\circ/90^\circ$ and $230^\circ/270^\circ$.

The discovery by Leinert, Haas, & Weitzel (1993) of a light scattering “halo” $\sim 1''$ in size around LkH α 233 led them to suggest that the star is highly embedded and optically visible largely through scattered light. Corcoran & Ray (1998) discovered a bipolar jet and counterjet (HH 398) spectroscopically at P.A.s of approximately 245° and 65° that bisect the X-shaped nebula. In their spectrograms, the redshifted counterjet is seen to begin $0''.7$ from the centre of the stellar continuum, whereas the blueshifted jet can be traced right back to the continuum peak. The jet, and counterjet, can be seen in our continuum subtracted image (Fig. 12) along with a number of HH objects along the outflow direction.

Evidence for the presence of a large “polarisation disk” centred on LkH α 233 with a radius of about 15000 AU was found by Aspin, McCaughrean, & McLean (1985). The position angle of this disk is about 155° , which places it perpendicular to the observed optical outflow. The existence of this “polarisation disk” combined with the fact that the counterjet is not seen spectroscopically close to the star leads to the conclusion that there is a circumstellar disk present that obscures the beginning of the receding flow.

Close to LkH α 233 the [SII] emission can be resolved into two velocity components (Corcoran & Ray, 1998). The high velocity component is identified with the optical jet while the low velocity component, which extends to less than $2''$ from the star, may be modelled as a rotationally broadened disk wind (see Kwan & Tadamaru, 1995).

This survey revealed a number of previously unknown HH objects in the vicinity of LkH α 233. It is possible that not all of these objects can be attributed to LkH α 233 and the positions of a nearby IRAS source, IRAS 22317+4024, complicates our analysis (see Fig. 10). Candidate driving sources for all the new HH objects are suggested here.

Continuum subtracted images of the nebula surrounding LkH α 233 reveal a number of HH features which are not seen, at least so clearly, in the [SII] image alone. Fig. 12 shows the first optical images of an $\sim 7''$ jet emerging from the LkH α 233 nebula at a P.A. of $\sim 248^\circ$, which is relatively close to the P.A. of the jet as spectroscopically determined by Corcoran & Ray (1998). A possible counterjet to the northeast of LkH α 233 is also seen in this image. But it is difficult to determine whether this is actually a counterjet or simply a residual of the continuum

subtraction process. There are two other emission knots to the southwest of the source. The first of these, HH 808, is situated close to a diffraction spike from a bright star to the west of LkH α 233. HH 808 is 1'.05 from the source at a P.A. of 250°. The second knot, HH 809, is 2'.2 from the source at a P.A. of 241°. Two other objects were seen to the northeast of LkH α 233 at a distance of \sim 2', the first has a P.A. of 63° and the second is at 65°. These objects are outside the area shown in Fig. 12 and it is unclear at present whether these are HH objects.

Also to the northeast of LkH α 233, we discovered HH 814 (Fig. 10) at a distance of 5'.18 (1.3 pc). The morphology of this object may be studied more clearly in the continuum subtracted image inset in Fig. 10. HH 814 appears to be a broad bow shock facing back towards LkH α 233 at a P.A. of 47° with respect to LkH α 233. Corcoran & Ray (1998) determined a P.A. of approximately 65° for the counterjet, suggesting that if HH 814 is part of the same flow, its direction has changed by \sim 20°. Note however that the P.A. determined by Corcoran & Ray (1998) is very crude as it was deduced by slit sampling at various P.A.'s.

A number of other objects were discovered to the southwest of LkH α 233 (see Fig. 11). HH 810, HH 811 and HH 812, are at 4'.5 (1.2 pc), 6' (1.5 pc) and 6'.5 (1.7 pc) respectively from LkH α 233, all at a P.A. of 236°. HH 813, at a distance of 7' (1.8 pc) has a P.A. of 247° with respect to LkH α 233. Considering the possibility that outflows from higher mass stars may not be as collimated as those from low mass stars, HH 810- HH 814 could be the optical tracers of the edges of a moderately collimated flow driven by LkH α 233. The axis of this outflow with respect to LkH α 233 is \sim 62° (marked on Fig. 10), which agrees well with the estimate of the P.A. of the jet closer to the source. It is also possible that HH 813 is a bow shock facing back towards IRAS 22317+4024 (Fig. 11). Proper motion studies could conclusively determine whether this is the case.

3.5. The NGC 7129 region

A large number of YSOs are known in the NGC 7129 cluster which lies at a distance of 1.25 kpc (Shevchenko & Yakubov, 1989). Aside from optically visible young stars such as LkH α 234, there are many embedded ones. For example, a 160 μ m survey by Bechis et al. (1978) revealed two far infrared sources and although one of them is spatially coincident with LkH α 234 (FIRS 1), the other is 3' further south (FIRS 2) and optically invisible. Additional infrared (Weintraub, Kastner, & Mahesh, 1994; Cabrit, et al., 1997) and sub-millimetre sources (Fuente et al., 2001) are also known.

Associated with these sources one finds the usual host of phenomena typical of star formation including reflection nebulae (Bertout, 1987), molecular outflows (Edwards & Snell, 1983; Bertout, 1987;

Mitchell & Matthews, 1994), HH objects (Ray, 1987; Miranda, Eiroa, & Gomez de Castro, 1993), HH jets (Ray, 1987; Ray et al., 1990; Cabrit, et al., 1997) and shocked H₂ flows (Eislöffel, 2000).

Looking at the distribution of previously known HH objects in the region, and the new ones discovered here (see below), one gets the impression (see Figs. 13 and 14) that the primary outflow axis, or axes, is roughly in a northeast to southwest direction and centred on the cluster core. Caution however is necessary. Proper motions studies have shown that some HH objects like GGD 32 and HH 103 are not moving to the southwest, as one might suspect, but instead to the west (Ray et al., 1990). Moreover others, like GGD 34 (Gómez de Castro & Robles, 1999) and possibly GGD 33 (Cohen & Schwartz, 1983; Goodrich, 1986), have their own sources outside the cluster core.

The HH 815 complex (Fig. 15) is over 1' in size and is at a distance of 11' (4 pc) from LkH α 234. The three emission regions in HH 815 (A, B and C) appear to form the edges of a large bow shock that is concave towards the cluster core. HH 816 (Fig. 16) may be another bow trailed by a series of faint HH knots i.e. HH 817- HH 820. HH 821, \sim 15" north of GGD 35, is aligned with HH 819 and HH 816 and so could form part of the same flow. We note also that HH 105, is on the same axis from the cluster core and that no source for HH 105, at least in its immediate vicinity, is known.

The most distant HH object to the southwest of the cluster discovered by us is HH 822 (Fig. 17). It is at a P.A. of 238° with respect to LkH α 234 and the morphology of its brightest component (HH 822 A), i.e. a bow concave towards the cluster, suggests it is part of an outflow that originated there. An additional knot close to HH 103 was also found and we shall refer to it as HH 103 A (Fig. 13). Given its location, it seems likely it is part of the same flow that drives HH 822. Moreover faint emission can be seen linking HH 103 A to HH 822 A reinforcing this conclusion. Finally we add that HH 822 B is at a distance of 10'.7 (3.9 pc) from LkH α 234.

The large number of sources in this region makes it extremely difficult, without detailed kinematic studies, to determine the origin of individual HH complexes. As previously mentioned there are a number of low mass YSOs, like the one that drives GGD 34, present and this complicates our analysis. That said, it seems likely, purely on morphological grounds as well as location, that many of the newly discovered HH objects are driven by a source(s) in the cluster core. Because of their large distance from the core, however, it may prove impossible, even with good proper motion data, to determine their precise origin. Several possible candidates exist including LkH α 234, IRS 6 and FIRS 1- MM1. If we draw an imaginary axis through the core at a P.A. of 60°/240° it roughly delineates the region where most of the new HH objects, HH 816 to HH 822, are located. Assuming we are dealing with one outflow here, that originates in the core, then its overall angular size is 21'.8 i.e. \sim 8 pc in projected length.

There are three other HH objects which are not situated along the major axis marked in Fig. 13. HH 824 and HH 825 are located on either side of IRAS 21416+6556 at $143^\circ / 323^\circ$ with respect to this source, suggesting a possible bipolar outflow driven by IRAS 21416+6556. These objects are $2'$ and $51''$ respectively from IRAS 21416+6556. The driving source of HH 823 is unclear as is its association with any of the other outflows in this region.

4. Discussion

4.1. Overall lengths

It has been stated, albeit somewhat tongue-in-cheek, that the apparent length of optical outflows from YSOs used to be a function of CCD chip size! Early chips were small and sampled only a small angular patch of the sky. This, in combination with the episodic nature of the flows themselves, conspired to suggest outflow lengths measured in tens of thousands of AU rather than parsecs. In a number of cases however CCD mosaicing (Ray, 1987) did hint that some flows were at least in the parsec league. Large format CCDs in focal-plane mosaics can cover fields of view larger than $30'$ which, at a distance of 1kpc, corresponds to more than 8.7pc. Flows can therefore be detected to beyond the peripheries of their parent cloud.

Table 2 lists parameters such as distance, source luminosity, outflow length, cloud size and degree of collimation for both the intermediate-mass sources discussed here and several well-studied outflows powered by both intermediate- and low-mass YSOs. In some regions, the projected lengths of the outflows are similar to the sizes of the clouds from which they emerge. This correlation of length scales is to be expected and there should also be a tendency for shocks to be seen near the cloud edges where extinction by dust is minimal.

If we assume an average tangential velocity for outflows of 100 km s^{-1} , in 10^5 yrs material originally at the source will be transported ~ 10 pc i.e. typically to the edge of the clouds we are studying. Using the evolutionary tracks of Palla & Stahler (1993), we see that such a period corresponds to about 10% of the time an average Herbig Ae/Be star spends in the pre-main sequence phase. It follows that only in the case of the more massive YSOs, i.e. those with the shortest evolutionary timescales, do HH outflows represent a “fossil record” of activity over the totality of the outflow phase.

4.2. Morphology

HH outflows are episodic: they are clearly not continuous phenomena. For the most part, the shocks we see are generated by supersonic jet material ramming into previously ejected slower gas. This process produces a series of “working surfaces”, radiative shock systems that fade with time and therefore with distance from their source. Only the strongest shocks survive to produce dramatic, often chaotic, structures on parsec scales. It has even been

suggested that the FU Orionis phenomena may signal the dramatic change in output needed at the source to produce such a shock (Reipurth, 1989). Thus the spacing between HH objects increases with distance from the source at least amongst low mass YSOs (Reipurth & Bally, 2001). Such a trend is also visible here amongst the flows from intermediate mass YSOs such as LkH α 198 and 1548C27. Another phenomenon that occurs with HH outflows from low mass YSOs is that the shock structures become larger and apparently more chaotic with distance. Again this is something which is replicated in their intermediate mass YSO counterparts.

A phenomenon that is found in parsec-scale outflows from lower mass YSOs is that the flow often exhibits “S” or “C” shape symmetry (Reipurth, 1989) possibly as a result of jet precession or source motion through the parent cloud respectively. In our small sample, we do not find any clear-cut examples of either although, as previously mentioned, the parsec-scale outflow from 1548C27 IRS 1 may be “S-shaped”.

4.3. Collimation

As alluded to in the Introduction, one of the most striking differences between parsec-scale outflows from low and massive YSOs is the relative lack of collimation seen in the latter (Shepherd, Churchwell, & Wilner, 1997; Hunter, Phillips, & Menten, 1997; Shepherd, Watson, Sargent, & Churchwell, 1998). This point is well illustrated by the archetypal example of an outflow from a high luminosity YSO: the Orion IRC2 flow (Allen & Burton, 1993). Its opening angle is $\sim 90^\circ$ (Burton & Allen, 1994) which is a sharp contrast to the angles (typically a few degrees) seen in outflows from low-mass YSOs.

Table 2 list “final” opening angles for our small sample. Values are determined by dividing the width of the most distant HH object by its projected source separation. Note that as we are using projected separations the quoted values must be upper limits, however our observations only reveal the brightest portions of the shocks and fainter outer parts may be missed, so the opening angles may actually be greater than what is optically observed. Observed opening angles range from 0.9° to 12° suggesting a degree of collimation comparable to that seen in outflows from low-mass YSOs. This also suggests that the transition from well-collimated outflows to poorly-collimated outflows occurs at higher masses than the sources observed here.

4.4. The Frequency of Blow-outs

The true size of an outflow, in comparison to that of its parent cloud, is an important factor in determining whether the outflow’s energy and momentum is transported into the ISM or remains within the cloud itself. A cursory examination of our data shows a clear tendency

Source	Distance (pc)	Ref.	L_{bol} / L_{\odot}	Ref.	Outflow length (pc)	Ref.	Associated Cloud	Cloud size ^a (pc)	θ_{flow} ^b ($^{\circ}$)
LkH α 198	600	2	≥ 160	2	2.3	1	L1265	2	2.8
1548C27 IRS 1	2400	3	580	3	7.5	1	NGC 6823	33	11.6
IRAS 19395+2313	2400	3	320	1	5	1	NGC 6823	33	30.2
LkH α 233	880	4	≥ 121	4	3.1	1	ANON	3.2	6.3
LkH α 234	1250	5	1200	6	8	1	NGC 7129	5.1	6.2
IRAS 18162 - 2048 ^c	1700	7	1700	8	5.3	8	L291	15	1
HH 354 IRS	750	9	120	9	2.4	10	L1165	1.8	4.04
PV Cephei	500	11	100	12	2.6	10,13	L1617	28	6.7
IRAS 05491+0247 ^{d,e}	460	10	25	10	7.7	10	L1617	28	7.4
HH 1/2 VLA 1 ^e	460	14	50	15	5.9	16	L1641	25	10.3
HH 34 IRS ^e	460	14	28	17	3	18	L1641	25	1.5

Table 2. Parameters of newly discovered, and some previously known, parsec-scale outflows from low- and intermediate-mass YSOs.

^a : This is the diameter of the cloud where diameter = [major axis + minor axis]/2

^b : θ_{flow} is calculated by taking the width of the most distant shock in both the outflow and counterflow and dividing by the projected distance from the source. The mean value of θ_{flow} for the outflow and counterflow is given here.

^c : The source of HH 80 / HH 81.

^d : The source of HH 111.

^e : These YSOs are low-mass sources and are included here for comparison purposes only.

References : 1. this paper; 2. Chavarría-K. (1985); 3. Dent & Aspin (1992); 4. Calvet & Cohen (1978); 5. Shevchenko & Yakubov (1989); 6. Harvey, Wilking, & Joy (1984); 7. Rodriguez, Moran, & Ho (1980); 8. Martí, Rodriguez, & Reipurth (1993); 9. Schwartz, Wilking, & Giulbudagian (1991); 10. Reipurth, Bally, & Devine (1997); 11. Cohen, Kuhl, Spinrad, & Harlan (1981); 12. Mundt & Ray (1994); 13. Gomez, Kenyon, & Whitney (1997); 14. Hester, Stapelfeldt, & Scowen (1998); 15. Harvey, Joy, Lester, & Wilking (1986); 16. Ogura (1995); 17. Reipurth et al. (1993); 18. Bally & Devine (1994)

for HH objects to lie close to the edges of the parent cloud or at least close to the edges of clumps. As already mentioned, such an effect is to be expected considering the low extinction near cloud peripheries and the very low ISM densities beyond the cloud boundaries.

More importantly, it is clear that actual outflow timescales are very long in comparison to apparent dynamical ones. Here dynamical timescales are derived by dividing the projected length of an outflow by its estimated tangential velocity. This, and the observation of HH objects near cloud boundaries, immediately suggests that most, if not all, of the flows studied here have blown-out of their parent cloud.

4.5. Are outflows a source of cloud turbulence?

There is plenty of evidence to suggest molecular clouds are turbulent (Ward-Thompson 2002 and references therein) and that the pressure generated by this turbulence is sufficient to prevent clouds from collapsing under their own gravity. It has been shown however that cloud turbulence, even in the presence of magnetic fields, decays too quickly compared to typical cloud lifetimes (Stone, Ostriker, & Gammie, 1998) and must therefore be somehow replenished. Could outflows be the primary source of turbulence in molecular clouds?

The parsec-scale HH outflows imaged here appear largely well-collimated and therefore one might think they could affect only a narrow cone of ambient material. One

has to remember however that these flows are supersonic and that we are viewing only the most highly collimated outflow component. The same flows “imaged” in the CO J = 1 \rightarrow 0 line would normally appear much less collimated, especially at low velocities. That these flows affect cloud structure on parsec scales is evident from features such as the large CO “cavity” in NGC 7129. No doubt they also affect cloud dynamics. Arce & Goodman (2001) for example has found that molecular outflows associated with parsec-scale HH flows can possess kinetic energies comparable to the turbulent and gravitational binding energies of their parent clouds. This proves however only that they are a potentially important source of turbulence. Unfortunately we do not understand the coupling between outflows and their ambient medium well enough to be sure. Numerical simulations (Downes & Cabrit, 2003) are helping to address this problem but further studies are required.

5. Conclusions

We have investigated the occurrence of parsec-scale outflows from intermediate-mass YSOs. As is the case with lower mass YSOs, such flows appear to be common and we report the discovery of four here with well defined sources. These include LkH α 198, 1548C27 IRS 1, LkH α 233 and IRAS 19395+2313. All of these YSOs, with the exception of the last, were previously known to have small-scale outflow activity.

The region surrounding the Herbig Ae star LkH α 234 is cluttered with outflows and candidate sources. Twelve new HH objects are reported on here, with many of them lying along a preferential axis centred near LkH α 234 and orientated in a northeast-southwest direction. Their morphology suggests that at least some are part of a large-scale flow centred on the core of the NGC 7129 cluster.

Parsec-scale outflows from intermediate-mass YSOs show a number of similarities to those from their low-mass counterparts. In particular :

- their lengths and degree of collimation appear comparable,
- they share the same morphological trends such as decreasing frequency, increasing dimension and increasing complexity of HH emission with distance from the source.

The lengths of these large-scale outflows are usually comparable to the clump size of their associated clouds. As their expected lifetimes are much larger than the apparent dynamical timescales, this suggests that many have “blown-out” of the cloud complex.

Finally, it is evident that the transition from highly collimated jet-like flows to poorly collimated wide-angle outflows such as OMC1 must lie at higher masses and luminosities than the sources studied here.

Acknowledgements. FMcG and TPR acknowledge support from Enterprise Ireland. JB's research was supported by NSF grant AST-9819820, NASA grant ANG5-8108 (LTSA), and NASA grant NCC2-1052 (CU Center for Astrobiology).

References

Allen, D. A. & Burton, M. G. 1993, *Nature*, 363, 54
 Alten, V. P., Bally, J., Devine, D., & Miller, G. J. 1997, *IAU Symp.* 182: Herbig-Haro Flows and the Birth of Stars, 182, 51P
 Arce, H. G. & Goodman, A. A. 2001, *ApJ*, 554, 132
 Aspin, C., McCaughrean, M. J., & McLean, I. S. 1985, *A&A*, 144, 220
 Aspin, C. & Reipurth, B. 2000, *MNRAS*, 311, 522
 Bally, J. & Devine, D. 1994, *ApJ*, 428, L65
 Bechis, K. P., Harvey, P. M., Campbell, M. F., & Hoffmann, W. F. 1978, *ApJ*, 226, 439
 Bertout, C. 1987, *IAU Symp.* 122: Circumstellar Matter, 122, 23
 Burton, M. G. & Allen, D. A. 1994, *ASSL Vol. 190: Astronomy with Arrays, The Next Generation*, 61
 Cabrit, S., Lagage, P. -, McCaughrean, M., & Olofsson, G. 1997, *A&A*, 321, 523
 Calvet, N. & Cohen, M. 1978, *MNRAS*, 182, 687
 Canto, J., Rodriguez, L. F., Calvet, N., & Levreault, R. M. 1984, *ApJ*, 282, 631
 Cohen, M., Kuhl, L. V., Spinrad, H., & Harlan, E. A. 1981, *ApJ*, 245, 920
 Cohen, M. & Schwartz, R. D. 1983, *ApJ*, 265, 877
 Chavarría-K., C. 1985, *A&A*, 148, 317
 Corcoran, D. & Ray, T. P. 1995, *A&A*, 301, 729
 Corcoran, M. & Ray, T. P. 1997, *A&A*, 321, 189
 Corcoran, M. & Ray, T. P. 1998, *A&A*, 336, 535

(CRB)
 Craine, E. R., Byard, P. L., & Boeshaar, G. O. 1981, *AJ*, 86, 751
 Downes, T. P. & Cabrit, S. 2003, *A&A*, 403, 135
 Dent, W. R. F. & Aspin, C. 1992, *MNRAS*, 259, 401
 Edwards, S. & Snell, R. L. 1983, *ApJ*, 270, 605
 Eiroa, C., Gomez de Castro, A. I., & Miranda, L. F. 1992, *A&AS*, 92, 721
 Eisloffel, J. & Mundt, R. 1997, *AJ*, 114, 280
 Eisloffel, J. 2000, *A&A*, 354, 236
 Fuente, A., Neri, R., Martín-Pintado, J., Bachiller, R., Rodríguez-Franco, A., & Palla, F. 2001, *A&A*, 366, 873
 Goodrich, R. W. 1986, *AJ*, 92, 885
 Goodrich, R. W. 1993, *ApJS*, 88, 609
 Gomez, M., Kenyon, S. J., & Whitney, B. A. 1997, *AJ*, 114, 265
 Gómez de Castro, A. I. & Robles, A. 1999, *A&A*, 344, 632
 Harvey, P. M., Wilking, B. A., & Joy, M. 1984, *ApJ*, 278, 156
 Harvey, P. M., Joy, M., Lester, D. F., & Wilking, B. A. 1986, *ApJ*, 301, 346
 Hartigan, P., Edwards, S., & Ghandour, L. 1995, *ApJ*, 452, 736
 Hartigan, P., Morse, J., & Bally, J. 2000, *AJ*, 120, 1436
 Heathcote, S., Morse, J. A., Hartigan, P., Reipurth, B., Schwartz, R. D., Bally, J., & Stone, J. M. 1996, *AJ*, 112, 1141
 Herbig, G. H. 1960, *ApJS*, 4, 337
 Hester, J. J., Stapelfeldt, K. R., & Scowen, P. A. 1998, *AJ*, 116, 372
 Hunter, T. R., Phillips, T. G., & Menten, K. M. 1997, *ApJ*, 478, 283
 Kwan, J. & Tadamaru, E. 1995, *ApJ*, 454, 382
 Lagage, P. O., Olofsson, G., Cabrit, S., Cesarsky, C. J., Nordh, L., & Rodriguez Espinosa, J. M. 1993, *ApJ*, 417, L79
 Leinert, C., Haas, M., & Weitzel, N. 1993, *A&A*, 271, 535
 Marti, J., Rodriguez, L. F., & Reipurth, B. 1993, *ApJ*, 416, 208
 Miranda, L. F., Eiroa, C., & Gomez de Castro, A. I. 1993, *A&A*, 271, 564
 Mitchell, G. F. & Matthews, H. E. 1994, *ApJ*, 423, L55
 Mundt, R. & Ray, T. P. 1994, *ASP Conf. Ser.* 62: The Nature and Evolutionary Status of Herbig Ae/Be Stars, 237
 Mundt, R., Bührke, T., Fried, J. W., Neckel, T., Sarcander, M., & Stocke, J. 1984, *A&A*, 140, 17
 Mundt, R., Brugel, E. W., & Bührke, T. 1987, *ApJ*, 319, 275
 O'Dell, C. R., Hartigan, P., Lane, W. M., Wong, S. K., Burton, M. G., Raymond, J., & Axon, D. J. 1997, *AJ*, 114, 730
 Ogura, K. 1995, *ApJ*, 450, L23
 Palla, F. & Stahler, S. W. 1993, *ApJ*, 418, 414
 Parthasarathy, M., Vijapurkar, J., & Drilling, J. S. 2000, *A&AS*, 145, 269.
 Phillips, J. P. & Mampaso, A. 1996, *A&A*, 316, 182
 Ray, T. P. 1987, *A&A*, 171, 145
 Ray, T. P., Poetzel, R., Solf, J., & Mundt, R. 1990, *ApJ*, 357, L45
 Reipurth, B. 1989, *Nature*, 340, 42
 Reipurth, B. & Bally, J. 2001, *ARA&A*, 39, 403
 Reipurth, B., Bally, J., & Devine, D. 1997, *AJ*, 114, 2708
 Reipurth, B., Chini, R., Krugel, E., Kreysa, E., & Sievers, A. 1993, *A&A*, 273, 221
 Rodriguez, L. F., Moran, J. M., & Ho, P. T. P. 1980, *ApJ*, 240, L149

Scarrott, S. M., Rolph, C. D., & Tadhunter, C. N. 1991, MNRAS, 249, 310

Schwartz, R. D., Wilking, B. A., & Giulbudagian, A. L. 1991, ApJ, 370, 263

Shepherd, D. S., Churchwell, E., & Wilner, D. J. 1997, ApJ, 482, 355

Shepherd, D. S., Watson, A. M., Sargent, A. I., & Churchwell, E. 1998, ApJ, 507, 861

Shevchenko, V. S. & Yakubov, S. D. 1989, Soviet Astronomy, 33, 370

Staude, H. J. & Elsasser, H. 1993, A&A Rev. , 5, 165

Stone, J. M., Ostriker, E. C., & Gammie, C. F. 1998, ApJ, 508, L99

Strom, K. M., Strom, S. E., Wenz, M., Wolff, S. C., & Morgan, J. 1986, ApJS, 62, 39

Vilchez, J. M., Mampaso, A., Riera, A., & Phillips, J. P. 1989, A&A, 213, 303

Ward-Thompson, D. 2002, Science, 295, 76

Weintraub, D. A., Kastner, J. H., & Mahesh, A. 1994, ApJ, 420, L87

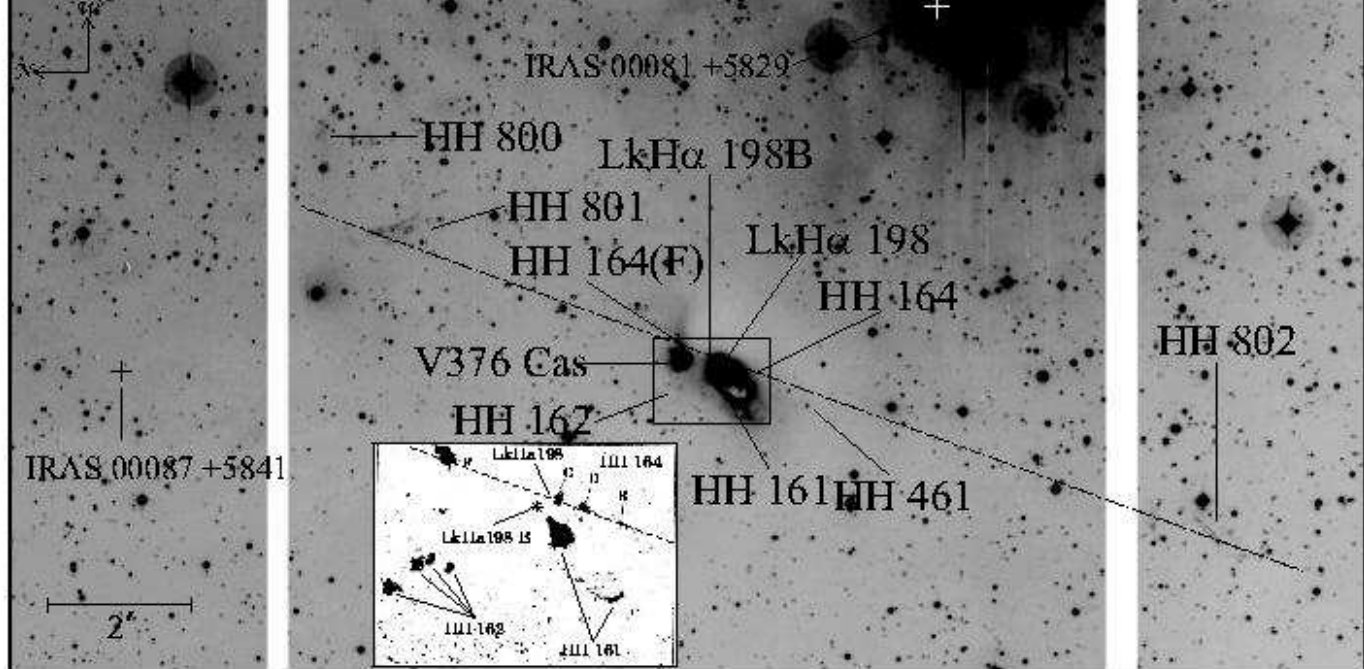


Fig. 1. *LkH α 198 [SII]* : Mosaic of the entire outflow around LkH α 198, including the three newly discovered HH complexes with the main outflow axis delineated by a dotted line. For all images relating to LkH α 198 (Figs. 1, 2 and 3) north is to the left and west to the top but for all subsequent images, north is to the top unless specified otherwise. The continuum subtracted [SII] image of Corcoran, Ray, & Bastien (1995) is inset, showing the HH 164 knots (C, D, E and F), most of which are not seen in our [SII] image due to the presence of the reflection nebula. Here, the position of LkH α 198 is indicated by a white cross slightly east of knot C. The P.A. of HH 164 at 340° (Corcoran, Ray, & Bastien, 1995) is marked on the inset and it can be seen from the outflow axis on the main image that the P.A. of the extended outflow is also at 340°. There are two known optically invisible IRAS sources in the region and their positions are marked. The white strips delineate gaps in the WFC CCD mosaic.

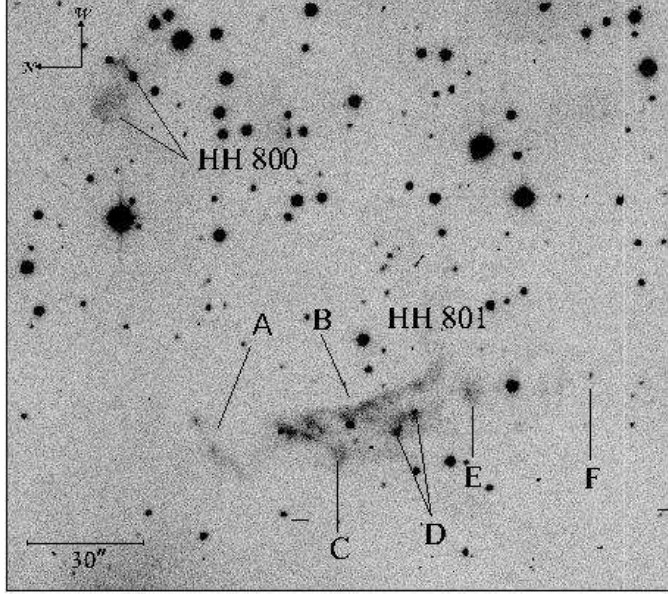


Fig. 2. *LkH α 198 [SII]* : HH 800 and HH 801 showing various features referred to in the text. The knotty morphology of HH 801 is clearly seen here.

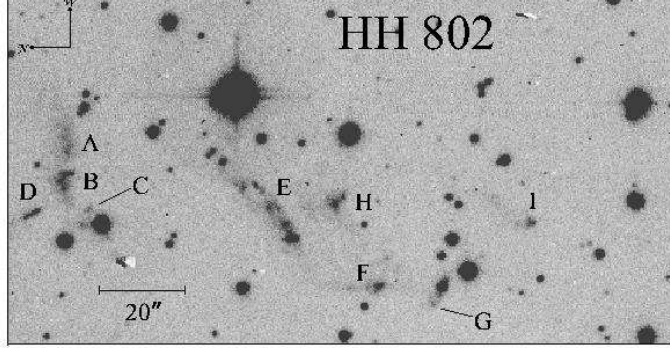


Fig. 3. *LkH α 198 [SII]* : HH 802, to the southeast of LkH α 198.

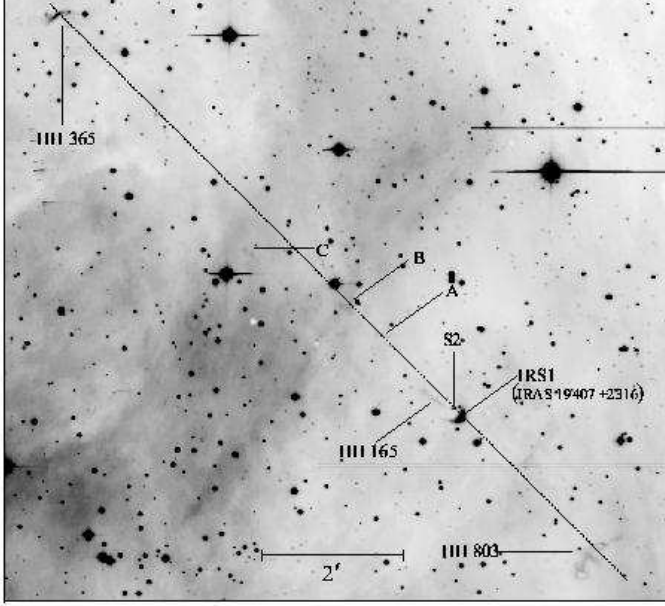


Fig. 4. *1548C27 H α* : Entire outflow around 1548C27IRS1. Note that north is to the top and east to the left in this and subsequent images. An approximate outflow axis is marked here, at a P.A. of $\sim 45^\circ$, however the outflow appears to be precessing – see text (section 3.2).

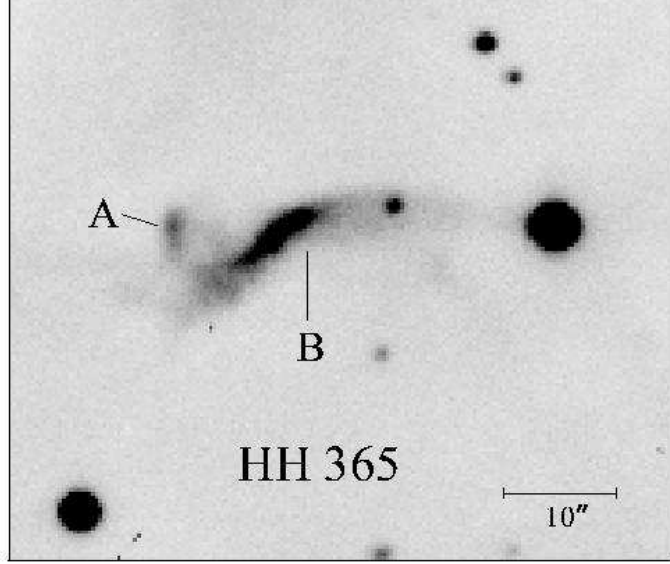


Fig. 5. *1548C27 H α* : HH365, to the northeast of 1548C27 IRS 1.

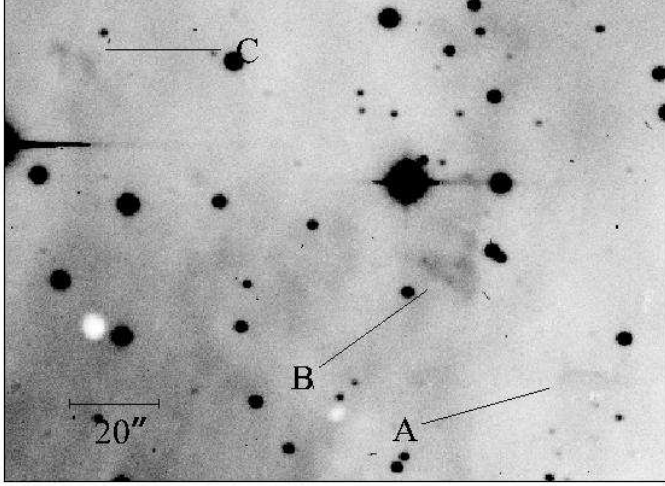


Fig. 6. *1548C27 H α* : Possible HH knots A, B and C to the northwest of HH165

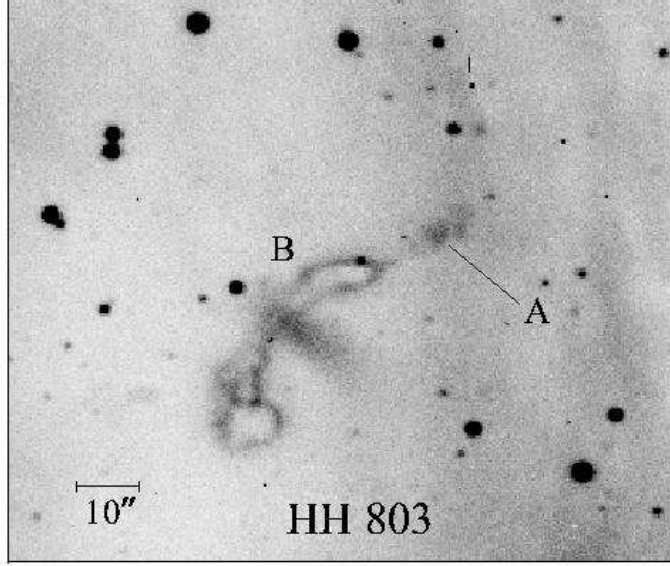


Fig. 7. *1548C27 H α* : The morphology of HH 803 is clearly seen in optical images.

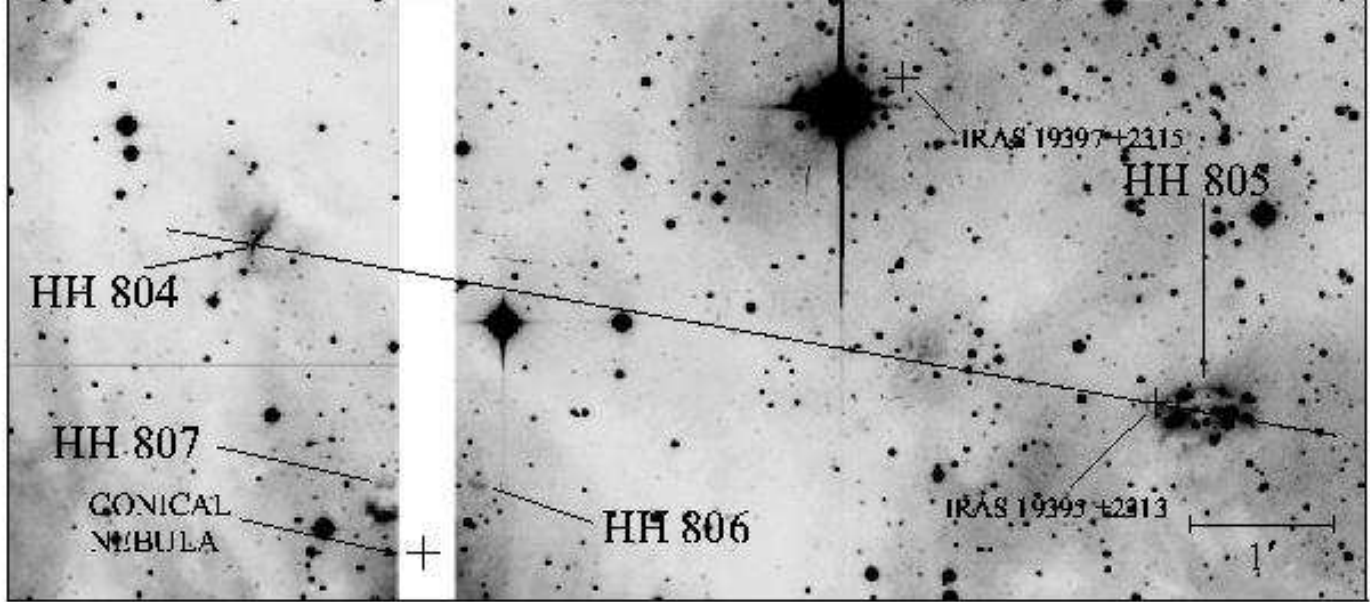


Fig. 8. *IRAS 19395+2313 H α* : The region around IRAS 19395+2313, including all known additional IRAS sources in its vicinity. Note that IRAS completeness at this distance is $\geq 100L_{\odot}$. Four newly discovered HH objects are marked. The position of the conical nebula, visible on the Palomar Sky Survey Red (E) plate and which might be associated with the driving source for HH 806, is indicated. The possible outflow from IRAS 19395+2313 is marked with a dotted line at a P.A. of 80° .

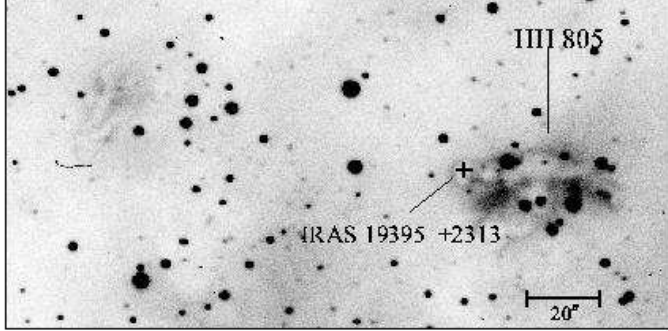


Fig. 9. *IRAS 19395+2313* $H\alpha$: HH 805 and its candidate driving source IRAS 19395+2313.

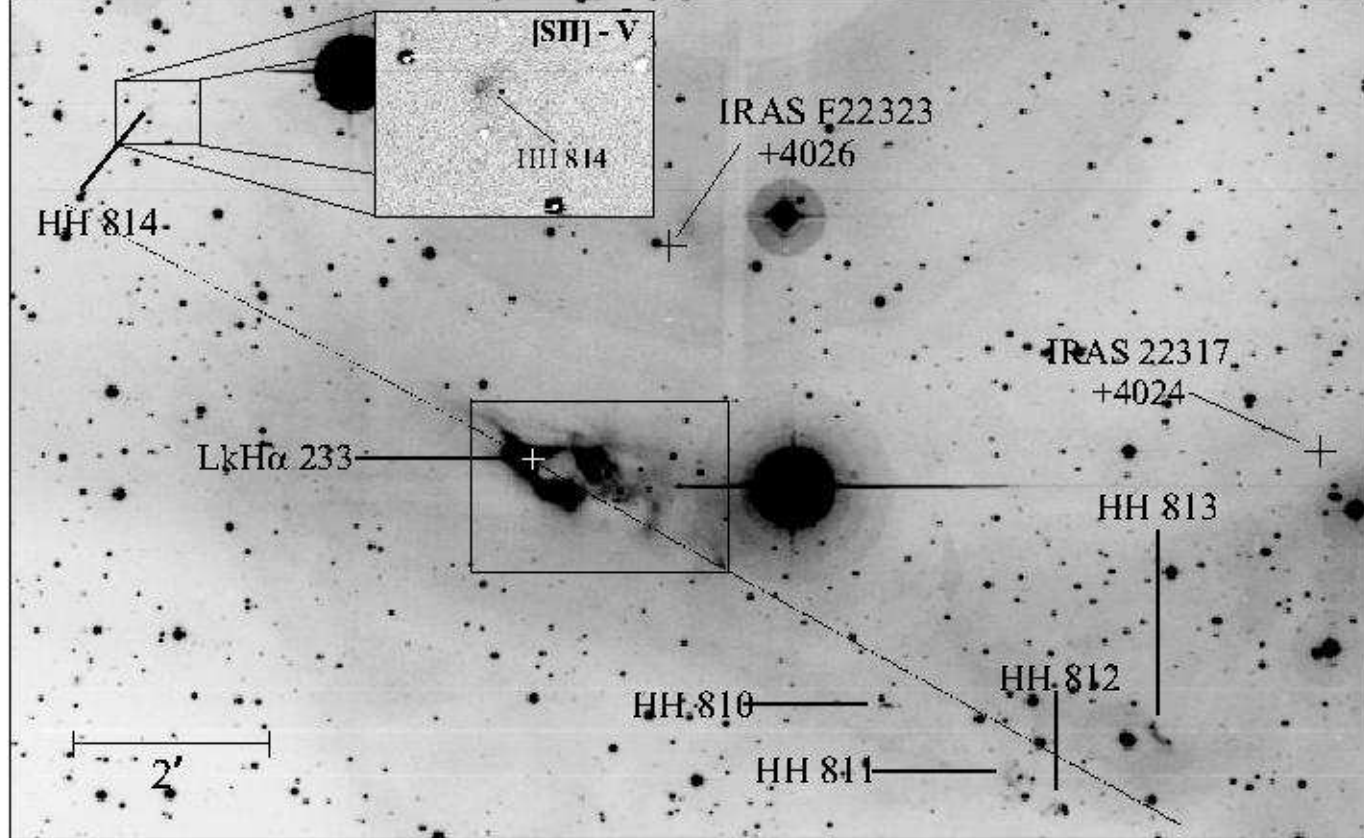


Fig. 10. *LkH α 233 [SII]* : The entire outflow around LkH α 233 including all known optically invisible IRAS sources in the region. The major axis of the outflow at 62° through the source is indicated by a straight line. The continuum subtracted ([SII]-V) image in the top right corner shows HH 814 more clearly. The area around LkH α 233 is marked by a box and is seen in more detail in Fig. 12.

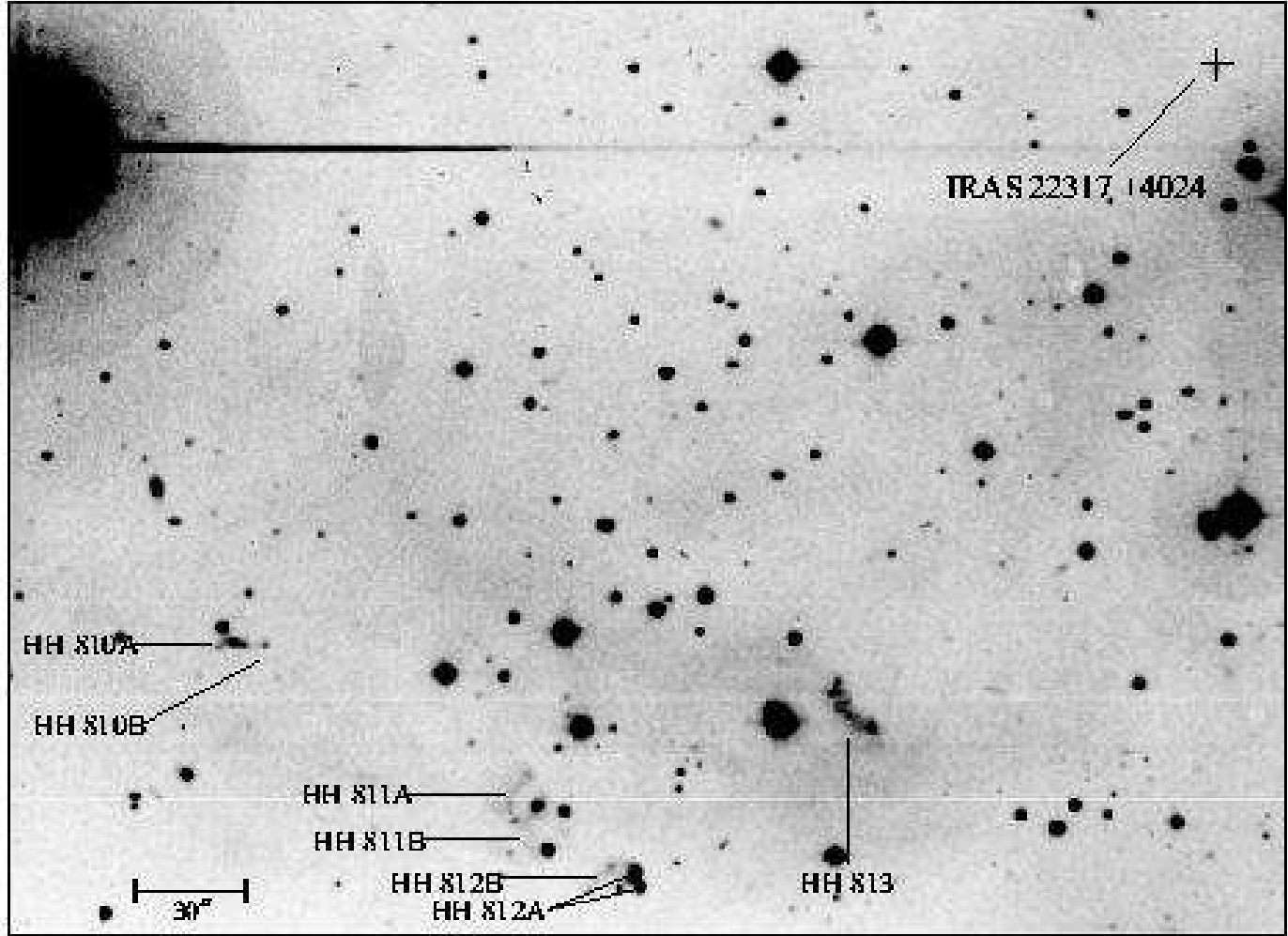


Fig. 11. $LkH\alpha$ 233 [SII]: HH 810–HH 813, to the southwest of $LkH\alpha$ 233.

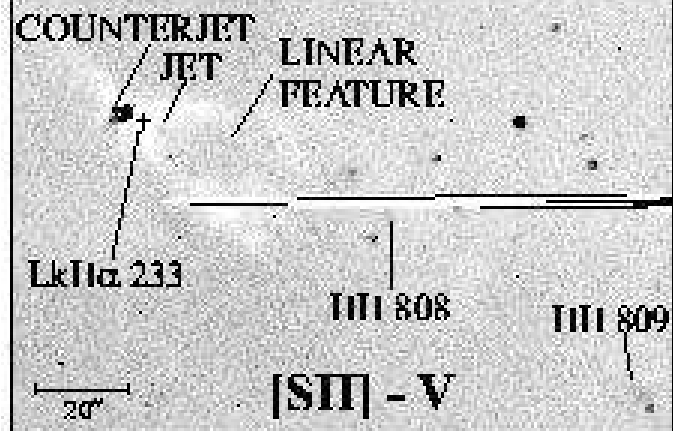


Fig. 12. *LkHa 233 [SII]*: Continuum subtracted image of the centre of the LkHa 233 nebula. The jet is optically visible here, along with a number of other emission features close to the source including HH 808 and HH 809.

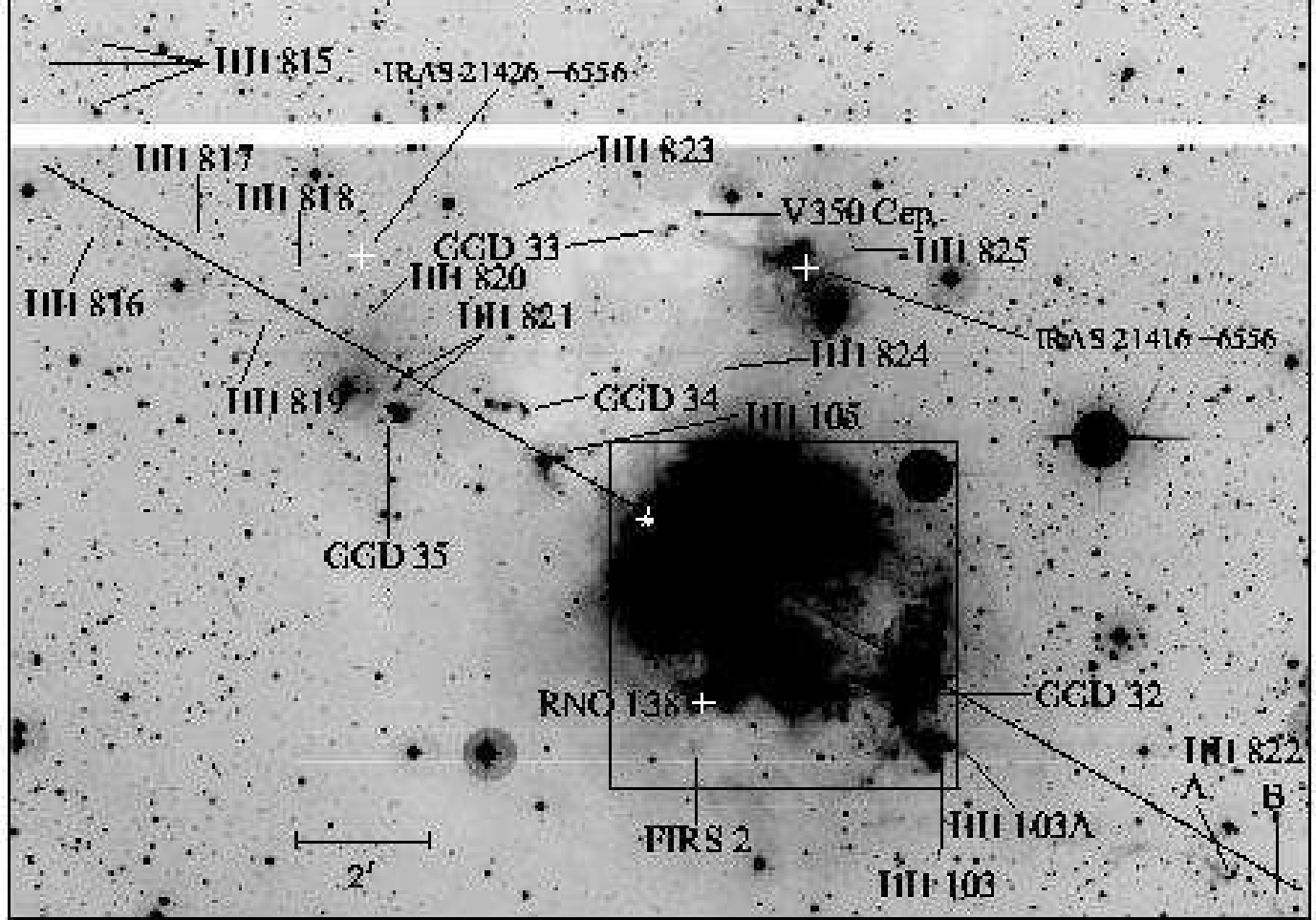


Fig. 13. *LkH α 234 [SII]*: Mosaic of the entire outflow around LkH α 234. The position of LkH α 234 is marked with a white star - the area surrounding LkH α 234 indicated by the box can be seen more clearly in Fig. 14. The dotted line marks the primary outflow axis flow at 60°/240°. There is an optically invisible IRAS source in the cluster, IRAS 21418+6552, the position of which is marked with a white cross in Fig. 14. Other known infrared sources in the region are also indicated.

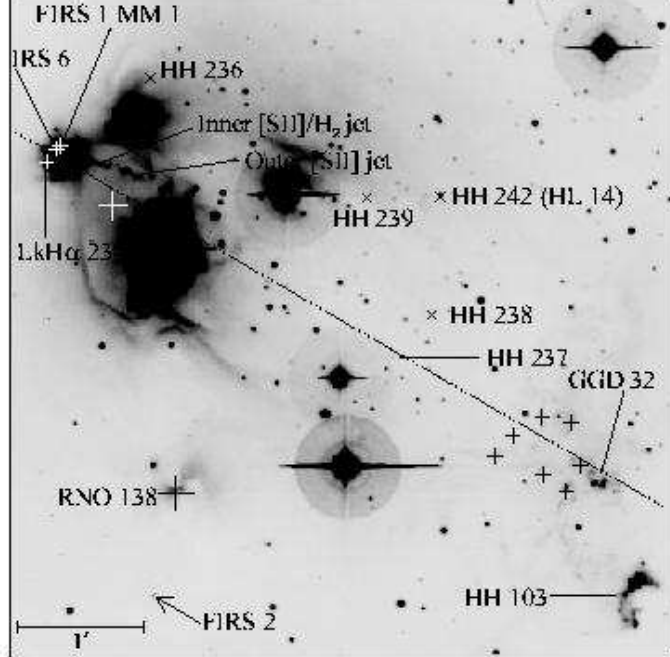


Fig. 14. *LkH α 234 [SII]* : The cluster region (indicated in Fig. 13) including the “inner” and “outer” optical jets (Ray et al., 1990; Cabrit, et al., 1997). The contrast has been changed here with respect to Fig. 13 so that more objects within the cluster core are visible. The white cross to the southwest of LkH α 234 marks the position of IRAS 21814+6552. Black crosses and X’s are used to mark the positions of HH objects found by Eiroa, Gomez de Castro, & Miranda (1992) and Miranda, Eiroa, & Gomez de Castro (1993) respectively. The apparent primary outflow axis through the cluster at 60°/240° is marked.

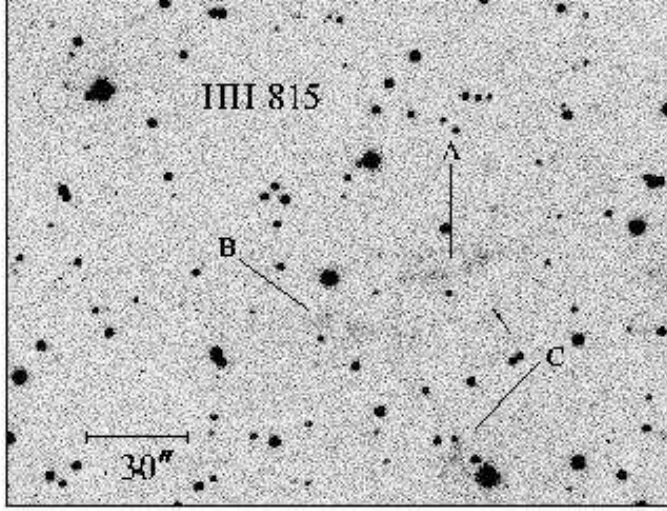


Fig. 15. *LkH α 234 [SII]*: HH 815, to the northeast of the cluster, is the most distant, known, outlying HH object in this region. Its relative position is seen in Fig. 13.

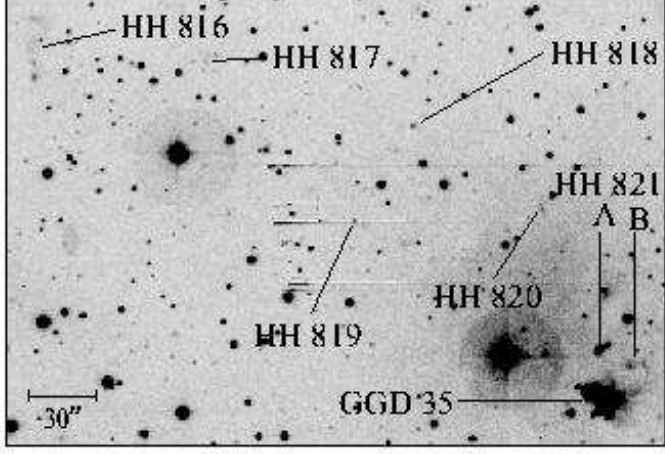


Fig. 16. *LkH α 234 [SII]*: HH 816 – HH 821 (A and B), to the northeast of *LkH α 234*.

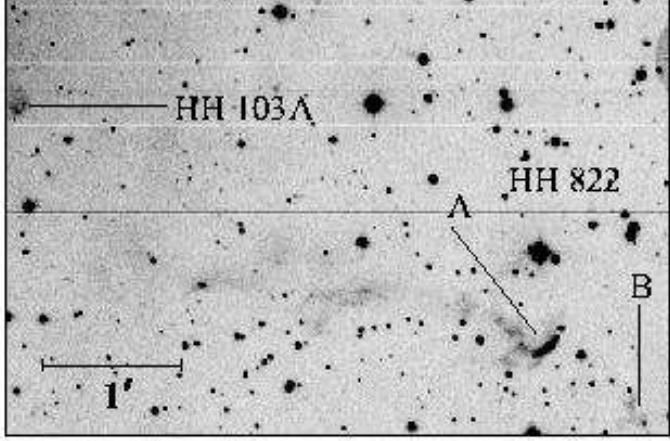


Fig. 17. *LkH α 234 [SII]* : HH103 A and HH822 to the southwest of LkH α 234.